

Influence of solution-annealing and stress-relieving on the pitting corrosion resistance of modified 316N SS weld metals: A study using EN technique

M.G. Pujar*, N. Parvathavarthini, R.K. Dayal

Corrosion Science and Technology Division, Indira Gandhi Centre for Atomic Research, Kalpakkam, Tamil Nadu 603102, India

ARTICLE INFO

Article history:

Received 29 July 2009

Received in revised form 23 March 2010

Accepted 25 April 2010

Keywords:

316LN Stainless steel

Welding

Microstructure

Pitting corrosion

Electrochemical noise

ABSTRACT

This paper presents the pitting corrosion resistance of AISI 316LN SS Weld joints in the (i) as-welded and (ii) post-weld heat-treated condition. The weld metal contains 0.055% carbon and 0.13% nitrogen in order to have improved creep strength. The welded components are subjected to (i) solution annealing at 1050 °C, (ii) stress relieving at 750 °C or (iii) dimensional stabilization at 550 °C depending upon the fabrication route. These welds are exposed to marine/coastal environment at various stages of fabrication, inspection, storage and commissioning after these heat-treatments, which may lead to pitting corrosion. Hence an attempt was made to understand the influence of microstructural change arising due to the post-weld heat-treatments on the susceptibility of these materials to pitting corrosion. Potentiodynamic polarisation as well as electrochemical noise (EN) studies were conducted in 0.5 M sodium chloride solution in open atmosphere. Shot-noise analysis, Weibull probability plots and the 3 dimensional plots using shot-noise parameters were used to assess the susceptibility to pitting corrosion. It has been established that solution annealing improves the pitting corrosion resistance whereas stress relieving as well as dimensional stabilization heat-treatments make the weld joints more prone to pitting. The localized corrosion resistance was correlated to the microstructural changes resulted during the various heat-treatments.

© 2010 Elsevier B.V. All rights reserved.

1. Introduction

AISI 316LN SS (C=0.024–0.03% and N=0.06–0.08%) has been chosen as the primary structural material for the 500 MWe Prototype Fast Breeder Reactor (PFBR) being built at Kalpakkam. Welding is extensively employed in the fabrication of PFBR components. For PFBR components welding of the AISI 316LN SS is to be carried out using modified 316N (as per AWS/ASME: SFA-5.4) electrodes developed indigenously. Weld metal cracking is controlled by optimizing the chemical composition of the welding consumables. Carbon in the range of 0.045–0.055% and nitrogen in the range of 0.06–0.1% are specified to provide weld joints with improved creep strength and freedom from sensitization in the as-welded state. In addition the ferrite content in the weld metal is specified to be between 3 and 7 FN (measured magnetically) to promote ferrite solidification mode.

Following three types of heat-treatments are required for austenitic stainless steel components [1]:

- (i) *Solution-annealing* at 1050 °C (1323 K) or above for full stress-relieving, restoration of mechanical properties and corrosion

resistance particularly when the maximum allowable level of cold work is exceeded. Following this treatment, slow cooling is necessary to avoid reintroduction of residual stress. When 316LN SS components (C ~ 0.03 wt.% and N ~ 0.08 wt.%) are welded with modified 316N electrodes (C ~ 0.045 to 0.055 wt.% and N ~ 0.06 to 0.1 wt.%), the carbon content of the weld metal will be higher than that of the base metal. When such high carbon weld metal is exposed to solution-annealing temperature, the delta-ferrite is transformed to austenite and the weld metal behaves like austenitic base metal containing higher carbon (~0.05 wt.% as against 0.03 wt.% in base metal).

- (ii) PFBR is a 'pool-type' of 500 MWe sodium-cooled reactor, wherein the minimum and maximum sodium temperatures in the secondary circuits would be 355–525 °C (628–798 K). Some components of PFBR encounter wear (adhesive or abrasive) due to sliding movement and erosion of the protective oxide film from their surfaces due to high velocity sodium. High operating temperatures coupled with high contact stresses could result in self-welding of the mating parts. Nickel base, cobalt-free hard facing is used for mating parts in most of the nuclear steam system components. *Stress-relieving* at 750–850 °C (1023–1123 K) is required after hard facing because of the high stresses built-up at the coating–substrate interface. Without this heat-treatment cracking of the coating can take place during in-service thermal cycling because of the

* Corresponding author.

E-mail address: pujar55@gmail.com (M.G. Pujar).

mismatch between the expansion coefficients of the hard face coating and stainless steel substrate.

- (iii) *Dimensional stabilization* treatment is required for relieving peak residual stresses and is performed before final machining to prevent distortion during final machining and assembly. It is performed at a temperature 50 °C above the expected peak transient temperature (the highest temperature the component is likely to experience for short duration of time during service). According to ASM hand book [2], heat-treatment periods of 3–4 h per 25 mm are used for dimensional stabilization treatment and 1 h/25 mm is used for solution-annealing treatment.

Among the various factors that affect the corrosion behaviour, microsegregation of alloying elements is found to be a prominent one [3]. Heat input and welding technique affect the solidification behaviour of weld metals, thereby affecting its corrosion performance [4]. Microsegregation of Cr and Mo during weld solidification and cooling in type 316 and type 316L weld metals has been extensively studied by a number of workers [5–9]. They concluded that the microsegregation of Cr and particularly Mo [6,7] was found to be much higher at the δ/γ interphase boundaries. The segregated Mo was reported to be more detrimental to uniform corrosion of high-alloyed austenitic stainless steels [10]. Presence of 2–10% of the delta-ferrite is considered as a prerequisite to avoid solidification cracking during welding [11]. But this ferrite was found to be attacked in certain corrosive media leading to component failures [12,13]. It was also reported that the surface lying dendrites were more prone to corrosion attack where Cr distribution at the δ/γ interphase was nonuniform [12]. From the literature cited above it can be inferred that the weld metal is a weaker section of the weldment [14] and an assessment of its corrosion behaviour is complicated by several factors.

It is well known that the delta-ferrite present in the weld deposits is transformed to several secondary phases after exposure at elevated temperatures. Although they are present in minor amounts, they can be detrimental to the corrosion properties of such weld metals. Such service-exposed weld joints may be attacked during the shutdown period or during cleaning. It has been reported that in the as-deposited specimens, the Cr- and Mo-rich delta-ferrite is not attacked by passive film breakdown. However, such preferential attack and subsequent breakdown takes place in the thermally aged weld metals as the depleted areas formed due to the decomposition of the delta-ferrite to $M_{23}C_6$ and intermetallics provide susceptible sites for pit nucleation and growth [15,16]. Since the welded and fabricated components are stored before being put in the service, there is every likelihood of initiation of localized corrosion like pitting or crevice corrosion in the coastal environment of Kalpakkam with high humidity and the presence of chlorides in water due to unforeseen contamination. The concentration of chlorides would increase significantly due to frequent wetting and drying conditions, which would pose a serious localized corrosion problem to the fabricated and stored components. Therefore in order to study the relative susceptibilities of the 316N weld metals with different microstructures resulting from different heat-treatments to pitting corrosion, experiments were conducted in 0.5 M NaCl solution in open atmosphere at open circuit potential (OCP) using EN technique.

2. Experimental

2.1. Weld joint preparation

Weld pads were prepared by Shielded Metal Arc Welding (SMAW) process using modified 316N electrodes (3.15 mm diameter) supplied by M/s. Mailam India Ltd., and the welding parameters used are detailed in Table 1. The chemical composition of the weld metals was analyzed using optical emission spectroscopy (Jobin Yvon

Table 1
Welding parameters for modified 316N SS weld metal.

No. of passes	Arc voltage (V)	Arc current (A)	Speed (mm min ⁻¹)	Heat input (J mm ⁻¹)
1	22–23	115–120	160	991
2	22–23	115–120	186	852
3–16	21–22	120–130	160	1008
17–26	21–22	130–140	290	600

make model JY-132 F) and the results are given in Table 2. Liquid penetrant and radiographic examinations were performed to ensure that the weld pads were free from porosity and defects. From these weld metals, cylindrical specimens (25 mm length, 10 mm diameter) were machined to conduct the corrosion studies.

2.2. Heat-treatments and delta-ferrite measurement

The weld metals were heat-treated at (1) 550 °C/4 h (Stabilization treatment), (2) 750 °C/1 h (stress relief) and (3) 1065 °C/1 h (solution annealing) and cooled at the rate of 200 °C h⁻¹. This cooling rate was chosen in order to avoid precipitation of carbides or any other phases. Delta-ferrite measurements were carried out using Ferritescope on the as-welded as well as heat-treated weld metal specimens. In order to study the morphology of the delta-ferrite, the weld metals in the (i) as-welded and (ii) as-welded and solution-annealed conditions were electrolytically etched at 2 V in 10% oxalic acid for 15 s. Heat-treated weld metals were etched in Modified Murakami reagent (30 g Potassium Ferricyanide + 30 g Potassium Hydroxide + 150 ml water, immersion in the boiling solution for 15–45 s). Thereafter the specimens were cleaned and observed under optical microscope.

2.3. Potentiodynamic anodic polarisation studies

In order to avoid crevice corrosion attack generally observed in the mounted specimens, cylindrical specimens drilled and tapped at one end were used in the present work. These specimens were polished up to fine diamond (1 μ m) on the curved surface and up to 1200 grit on the flat surfaces. Since pit nucleation depends upon the passive film which in turn is dependent upon the surface finish, diamond finish of the curved surface will reduce the possibility of pit nucleation on the curved surface; thus pits would be preferentially nucleated on the flat surface, which would be helpful in studying the pit nucleation sites as well as pit morphology using optical microscope. Care was taken to round of the sharp edges in order to avoid the edge attack. The specimens were washed in soap solution and cleaned ultrasonically in methanol and dried before immersing in the solution. The specimen was immersed in the solution such that only the flat surface remained inside the solution avoiding the immersion of the curved surface. The anodic polarisation experiments were performed in five-necked polarisation cell with a luggin-haber probe and a salt-bridge in order to establish the contact of the working electrode with the reference electrode. All solutions were prepared using double-distilled water. All the experiments were performed in the aerated solution of 0.5 M NaCl. All the potentials were measured against saturated calomel electrode (SCE). Two platinum foils (with an area of 1 cm² each) spot-welded to the platinum wires were used as the counter electrode and were placed symmetrically on the opposite sides of the working electrode. The scan rate was chosen to be 0.1667 mV min⁻¹. Initially, the specimen was immersed in the solution for 45 min in order to observe the stable open circuit potential. After this period, anodic polarisation experiments were conducted from OCP till the specimen underwent stable pitting attack which was noticed by the monotonic rise in the current. Solartron SI 1287 Electrochemical Interface was used to conduct all the experi-

Table 2
Chemical composition of the weld metal, wt.%.

Element	wt.%
Carbon	0.055
Nitrogen	0.13
Chromium	18.3
Nickel	11.3
Molybdenum	1.8
Manganese	1.4
Silicon	0.32
Sulphur	0.008
Phosphorus	0.025
Tantalum	<0.01
Titanium	13 ppm
Niobium	<0.07
Vanadium	0.07
Boron	<10 ppm
Copper	0.08
Cobalt	0.07

ments. Optical microscopic studies were conducted after the anodic polarisation experiments.

2.4. Electrochemical noise studies

Electrochemical noise studies on these materials were performed using two nominally identical cylindrical specimens with the same chemical composition as well as metallurgical history. The specimens were connected to the EN measurement system (Solartron SI 1287) using threaded specimen rods, which were covered with Teflon tape. The specimens were polished up to 1200 grit finish, washed in soap water and degreased and ultrasonically cleaned in methanol. Potential and current noise measurements were performed by shorting together two identical working electrodes. The current flowing between the two working electrodes, as well as the potential between the working electrode and a reference electrode were monitored. The area of the specimen exposed to the solution was about 1.534 cm².

The potentiostat, which can perform this experiment actively, holds the working electrode connection at the 'ground' potential by a small amplifier circuit. If one 'working' electrode is directly connected to ground and the other is connected to the working electrode cable, they are both held at the same potential and are, in effect, 'shorted' together. Any current, which flows between the two electrodes, is measured by the instruments of current measurement circuits thus creating a Zero Resistance Ammeter (ZRA). The potential is measured between the 'working' electrodes (since they are shorted together, both 'working' electrodes are at the same potential) and a reference electrode. SCE was used as a reference electrode for the measurement of potential noise.

Electrochemical current and potential noise studies were conducted in aerated 0.5 M sodium chloride solutions at OCP and noise signals were collected at the sampling frequency of 1 Hz. Since in EN studies, the signal is mostly non-stationary, the drift or the trend gets introduced. Therefore, the drift or the trend removal was carried out using a suitable detrending technique, which is an accepted practice, before calculating the statistical parameters as well as power spectral density (PSD) values. Every day the EN data was collected for 21,600 s. All the potential and current noise data collected in the time domain were transformed in the frequency domain through the fast Fourier transform (FFT) method, by a dedicated software after suitably detrending.

2.5. Data analysis using stochastic theory and shot noise

Usually a large scatter is observed in the measurable parameters like corrosion rate, maximum pit depth, time to perforation etc. during localized corrosion. This scatter results from the influence of metal surface heterogeneities and from variations in the corrosive environment over time during pit growth. All these facts suggest that randomness is an inherent and unavoidable characteristic of pitting corrosion over time, so that stochastic models are better suited to describe pitting corrosion processes. The output obtained using the stochastic models is random or probabilistic. It may be possible to predict the generation probability of events in the future from the past events, which is termed as, "conditional probability" [17].

Shot-noise theory is based on the assumption that the current signal is composed of discrete charge carriers [18]. Shot noise is produced when the current takes the form of a series of statistically independent packets of charge, with each packet having a short duration [19]. The number of charge carriers passing a given point will be a random variable. According to the stochastic process the individual events are independent of other events, thus, shot-noise analysis is applicable to the individual events [18,19]. This theory can be applied to the analysis of electrochemical noise data from corrosion processes. If this theory is applied to EN, three parameters can be obtained: i_{corr} the average corrosion current, q the average charge in each event, and f_n frequency of the appearance of these events. Only two of these parameters are independent, since

$$i_{corr} = q \times f_n \quad (1)$$

It is not possible to measure i_{corr} , q and f_n directly, but it is possible to estimate them from the measured current and potential noise [20]. Assuming that shot noise is produced during breakdown of the passive film as well as pit initiation and hydrogen evolution, the q and f_n are given as [21]:

$$q = \frac{\sqrt{\text{PSD}_E \times \text{PSD}_I}}{B} \quad \text{and} \quad q = \frac{\sigma_I \sigma_V}{Bb} \quad (2)$$

$$f_n = \frac{B^2}{\text{PSD}_E \times A} \quad \text{and} \quad f_n = \frac{B^2 b}{\sigma_V^2} \quad (3)$$

where PSD_E and PSD_I are the low frequency PSD values of the potential and current noise respectively, B is the Stern–Geary coefficient, σ_I and σ_V are the standard deviation values of current and potential respectively and b is the bandwidth of measurement as, standard deviation is a function of measurement bandwidth and A is the surface area of the specimen. The charge q is independent of area and f_n is proportional to area, so it can be reported as events per second per unit area [20]. In these calculations the B value was not taken to be 0.026 V per decade as reported earlier [19]; B values were determined from the potentiodynamic anodic polarisation curves, as they differed considerably.

The cumulative probability $F(f_n)$ at each f_n is determined from the set of f_n values calculated using Eq. (3) given above according to the mean rank approximation [18]. According to this method (using f_n as an example): (1) all the values of f_n were sorted in an ascending order and (2) then the cumulative probability for each value was calculated as $M/(N+1)$, where M is the position in the sorted list, and N is the total number of entries in the list [18]. Similarly, the characteristic charge, q values were calculated as per the Eq. (2) and cumulative probability $F(q)$ was calculated at each q value.

Pit initiation time will follow a Weibull distribution [22] when it is regarded as the survival time defined as the time to first failure (passive film breakdown) of an individual part or process. Following this reasoning, the Weibull distribution is assumed as the distribution of the pit initiation times. Weibull distribution function is one of the frequently used cumulative probability functions for predicting life time in reliability test [17]. Using this distribution it is possible to analyze data even when two or more failure modes are present at the same time [23]. The Weibull distribution is often used in the field of life data analysis due to its flexibility—it can mimic the behaviour of other statistical distributions such as the normal and the exponential by modifying m parameter value as shown below. The cumulative probability $F(t)$ of a failure system can be written just as Weibull distribution function, which is expressed as [17],

$$F(t) = 1 - \exp\left(\frac{-t^m}{n}\right) \quad (4)$$

m and n are the shape and scale parameters, respectively; m is a dimensionless parameter and n is expressed as s^m . Shape parameters allow a distribution to take on a variety of shapes, depending on the value of the shape parameter. The Weibull distribution has a relatively simple distributional form. However, the shape parameter allows the Weibull to assume a wide variety of shapes. The effect of the scale parameter is to stretch out the graph. The Eq. (4) can be rewritten as follows:

$$\ln\left\{\ln\left[\frac{1}{1-F(t)}\right]\right\} = m \ln t - \ln n \quad (5)$$

By using the cumulative probability values for the localized corrosion events, f_n calculated previously, in the above equation and fitting, two parameters m and n can be determined from the slope of the linear plot of $\ln\{\ln[1/(1-F(t))]\}$ versus $\ln t$ (also known as Weibull probability plot) and from the intercept on the $\ln\{\ln[1/(1-F(t))]\}$ axis, respectively. In order to study the progress of pitting or passivation in these steels using Weibull probability plots, 100 data sets each consisting of 1024 EN data points were recorded continuously after 120 h immersion period. This was done in order to ensure that the steels either showed perfect passivation or metastable or stable pitting corrosion. These EN data points from these 100 data sets were detrended using linear detrending technique to calculate the shot-noise parameters given by Eqs. (2) and (3). Subsequently, Weibull probability plots were constructed to determine the mean-free time values for pit initiation.

3. Results and discussion

Alloys can solidify as primary ferrite or primary austenite, and still contain a rather small amount of ferrite at room temperature. The complexities of solidification are represented in a simplified way through the plots of chromium equivalent (Cr_{eq}) versus nickel equivalent (Ni_{eq}). $\text{Cr}_{eq}/\text{Ni}_{eq}$ values can be calculated as per the formulae given by Suuatala [24], DeLong [25] and WRC-92 [26]. These formulae are given below:

$$\text{Suuatala's formula} \rightarrow \text{Cr}_{eq}/\text{Ni}_{eq} = \frac{\text{Cr} + 1.37\text{Mo} + 1.5\text{Si} + 2\text{Nb} + 3\text{Ti}}{\text{Ni} + 0.31\text{Mn} + 22\text{C} + 14.2\text{N} + \text{Cu}} \quad (6)$$

$$\text{DeLong's formula} \rightarrow \text{Cr}_{eq}/\text{Ni}_{eq} = \frac{\text{Cr} + \text{Mo} + 1.5\text{Si} + 0.5\text{Nb}}{\text{Ni} + 0.5\text{Mn} + 30(\text{C} + \text{N})} \quad (7)$$

$$\text{WRC-1992 formula} \rightarrow \text{Cr}_{eq}/\text{Ni}_{eq} = \frac{\text{Cr} + \text{Mo} + 0.7\text{Nb}}{\text{Ni} + 35\text{C} + 20\text{N} + 0.25\text{Cu}} \quad (8)$$

The calculated values of the $\text{Cr}_{eq}/\text{Ni}_{eq}$ ratio using the above formulae were found to be 1.39 (Suuatala's formula), 1.17 (DeLong's formula) and 1.27 (WRC-1992 formula). Thus, as per the scheme of solidification given below, the mode of solidification for the weld metals with the $\text{Cr}_{eq}/\text{Ni}_{eq}$ ratios within the range of 1.25–1.48 is austeno-ferritic (AF) [27].



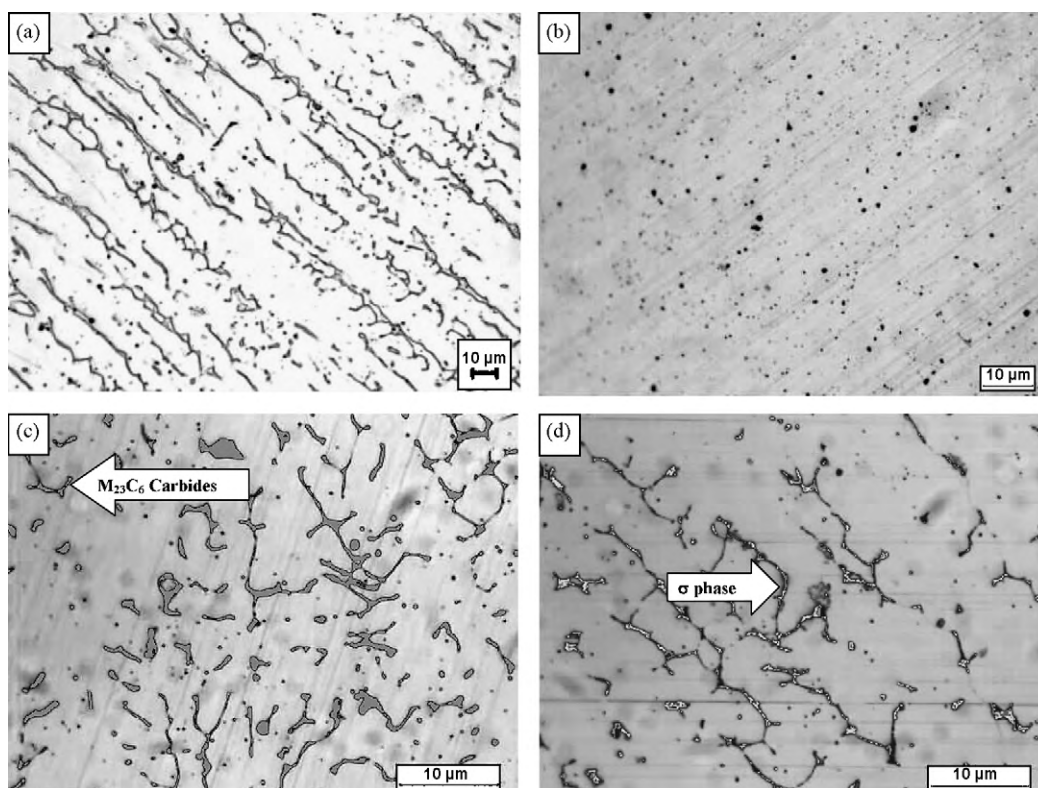


Fig. 1. The photomicrographs of 316N weld metal in as-welded (a), as-welded + SA (b) (electrochemically etched in 10% oxalic acid), heat-treated at 550 °C to 4 h (c) and 750 °C to 1 h (d) (etched in Modified Murakami reagent) conditions.

$$1.25 < \left(\frac{C_{\text{req}}}{N_{\text{req}}} \right) < 1.48 \quad (\text{AF mode})$$

The weld metals solidified in the austeno-ferritic mode. The microstructures of the as-welded as well as heat-treated weld metals are presented in Fig. 1a–d. Duplex austeno-ferritic structure with delta-ferrite with vermicular morphology can be clearly seen in the microstructure. Delta-ferrite content was estimated to be about 5.21 FN when measured using Ferritescope on the top bead. However, in some regions, nucleation of $M_{23}C_6$ carbides are expected in the as-welded condition itself on account of the exposure to the temperature range of 450–750 °C (723–1023 K) by thermal cycling during multipass welding. The heat-treatments given subsequently to the test specimens served to further transform the ferrite to various extents depending upon the temperature and time of exposure. The microstructure of the as-welded and solution-annealed specimens shows complete transformation of the delta-ferrite into the austenite, therefore the weld metal shows only the fine and round slag particles in the microstructure (Fig. 1b). When the weld metal is heat-treated at 550 °C to 4 h, delta-ferrite gets transformed to $M_{23}C_6$ carbides along the delta-ferrite/austenite (δ/γ) interphase boundaries. Thus, parts of the delta-ferrite stringers are seen to be decorated with fine $M_{23}C_6$ carbide particles with partial dissolution of the ferrite stringers (Fig. 1c). At 750 °C to 1 h, a large part of the delta-ferrite is transformed into the σ phase. The σ phase is clearly observed as reddish brown tinged particles at many places within the delta-ferrite phase. Any carbide precipitation that is observed is likely to have already formed during multipass welding, as it does not redissolve at this temperature. The grayish lines observed in the microstructures reveal the secondary austenite formed from the alloying-element depleted delta-ferrite after the precipitation of σ phase (Fig. 1d).

The potentiodynamic anodic polarisation curves for the 316N weld metals in as-welded and thermally aged condition are presented in Fig. 2. It was observed that the pitting potentials (E_{pp}) drastically became active on thermal ageing whereas the solution-annealed specimen showed remarkably very noble E_{pp} . The E_{pp} values as well as the B (Stern–Geary coefficient) values are presented in Table 3.

3.1. Electrochemical noise studies

The visual records of the current and the potential EN are shown in Fig. 3a–d. These records were obtained from the data logged on the third day of the exposure of the specimen to the medium and belong to the same time interval. It was observed that the cur-

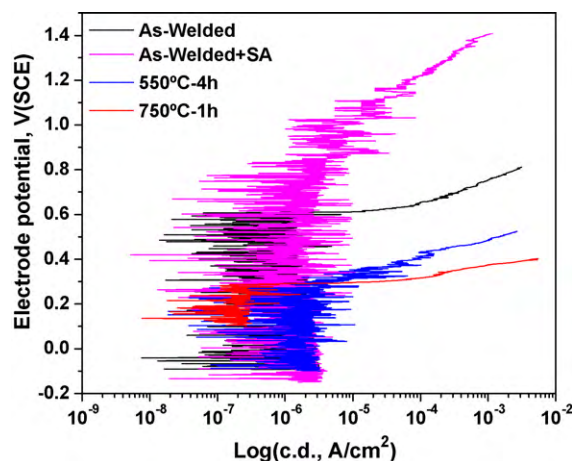


Fig. 2. Potentiodynamic anodic polarisation curves for 316N weld metal in as-welded and thermally aged condition in aerated 0.5 M NaCl solution.

Table 3
 E_{pp} and the B values for the 316N weld metals in aerated 0.5 M NaCl.

Weld metal specimen	E_{pp} (V (SCE))	B (V)
As-welded	0.61	0.0156
As-welded + SA	1.10	0.0790
550 °C to 4 h	0.40	0.0264
750 °C to 1 h	0.29	0.0024

rent noise amplitude was much lower in as-welded and as-welded and the solution-annealed specimen (in the range of -3×10^{-8} to 7×10^{-8} A), whereas the current transients for the thermally aged specimens (550 °C to 4 h) and (750 °C to 1 h) fall in the range of -3×10^{-7} to 1×10^{-8} A (Fig. 3c) and -4×10^{-7} to 1×10^{-6} A (Fig. 3d) respectively. The current noise signal in the specimen aged at 550 °C to 4 h showed a train of repetitive transients, which were almost equally spaced in time, indicating the growth and the repassivation of the metastable pits (Fig. 3b). In this case, since the pitting events were initiated on the second electrode, we could see the current and the potential signals in the same direction. Although, similar cyclic current transients were not observed in the specimen aged at 750 °C to 1 h, it showed potential transients dropping at regular intervals indicating the metastable pitting. This indicated repetitive breakdown and recovery of the passive film. Gonzalez-Rodriguez et al. [28] suggested that the generation of such noise signals was due to the action of the electrolyte on the bare surface. Henshall [29] reported that the observed fluctuations in electric current versus time response prior to the emergence of macroscopic pits could be attributed to the randomly occurring local passivity breakdown and repassivation events which

were precursors to the stable pit formation. A constant ennoblement of the potential signals in as-welded and as-welded and the solution-annealed specimens showed their tendency towards repassivation.

It is generally accepted that the breakdown of passive film (initiation of pitting corrosion) will cause a potential drop and a current rise at the same time, and the repassivation of passive film (repassivation of pitting corrosion) will cause the potential to increase and the current to decrease. Therefore, a new parameter called the corrosion admittance A_c is defined [30] as follows to reflect such events:

$$A_c = \frac{\Delta I}{\Delta V} \quad (9)$$

According to the Eq. (9), A_c is always negative if the working electrode is undergoing a process of initiation of localized corrosion or a process of repassivation. Therefore, A_c has three distinct states: positive, negative and zero. A positive value indicates that the working electrode is under uniform corrosion, a negative value indicates the initiation of localized corrosion. In this way all the corrosion activities (either localized or uniform corrosion) are clearly revealed in the A_c spectrum. A_c spectra were plotted for all the specimens using the data obtained after 48 h exposure period, the data consisting of 21,600 points (Fig. 4a–d). The as-welded specimen shows a slight indication of the localized attack, but as-welded and solution-annealed specimen shows excellent resistance to the localized attack. Among the thermally aged specimens, 550 °C to 4 h specimen showed clear indication of the localized corrosion attack whereas 750 °C to 1 h specimen showed extensive localized corrosion attack. Thus, although qualitative in nature, the relative

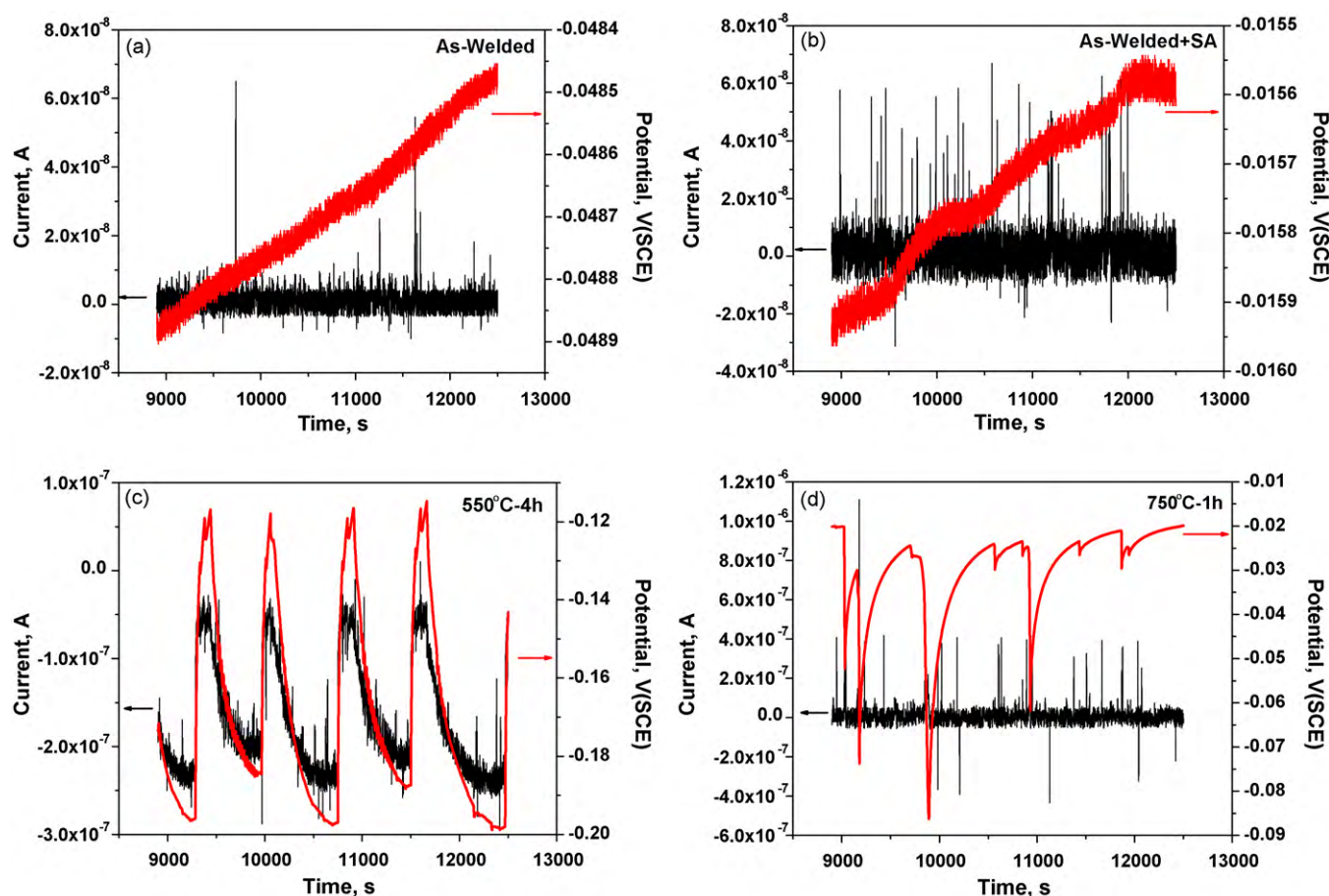


Fig. 3. Visual records of the current and the potential EN for specimens (immersed in 0.5 M NaCl) in as-welded (a), as-welded + SA (b), 550 °C to 4 h (c) and 750 °C to 1 h (d) condition.

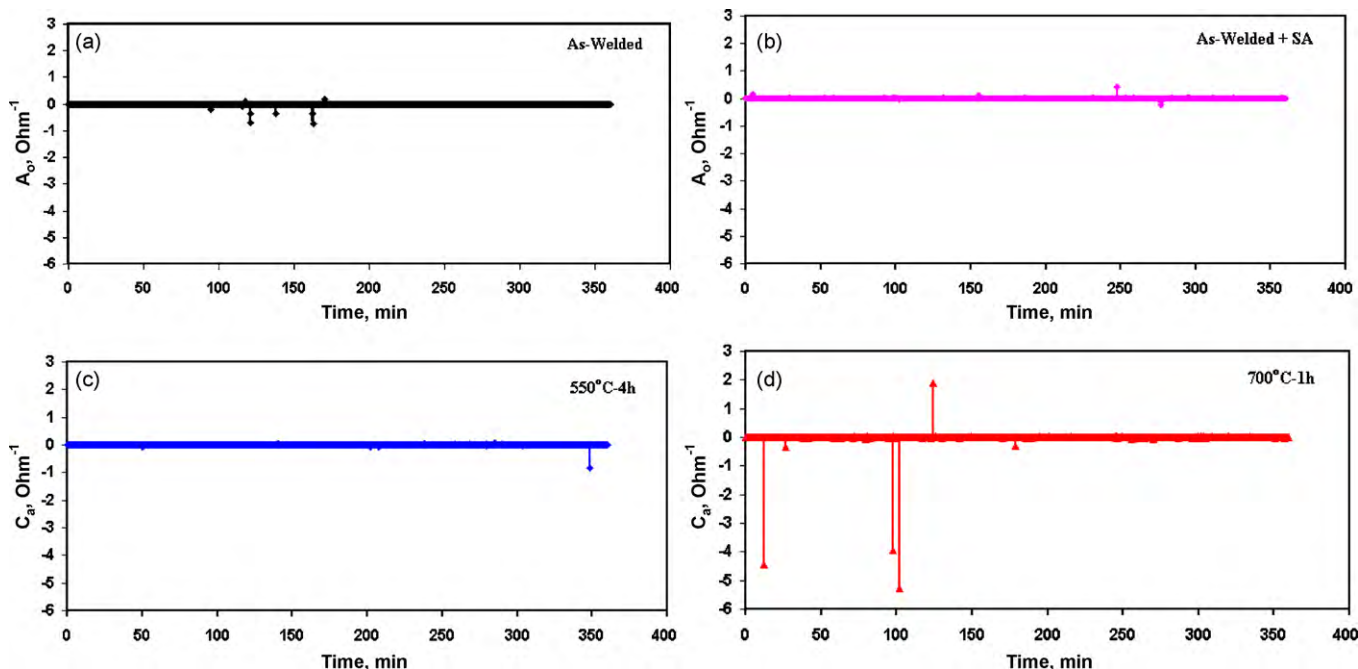


Fig. 4. Corrosion admittance plots for as-welded (a), as-welded + SA (b), 550 °C to 4 h (c) and 750 °C to 1 h (d) after 48 h of immersion in 0.5 M NaCl.

assessment of the pitting corrosion attack could be done quickly using corrosion admittance spectra.

For the analysis of a stochastic process like pitting corrosion, Weibull distribution plots are employed. In most of the stochastic models, small fluctuations in the local conditions (e.g. solution chemistry, fluid flow rate, surface topography, surface metallurgy) are envisioned to cause local breakdown of the passive film, resulting in the birth of the metastable pits also called as the “embryos.” Many of these embryos become unstable when the local conditions change and repassivation results. Once an embryo reaches a critical size or age, it becomes a “stable” pit and cannot die [29]. In the context of the present studies, Weibull distribution function was used to distinguish between uniform corrosion (in the passive state) and pitting corrosion and to investigate pitting corrosion alone in a quantitative way as reported earlier [31]. This type of EN data analysis was also used by Zhang et al. [32,33] to analyze their data on pure magnesium as well as magnesium alloys in thin electrolyte layers. Since the space of the distribution function should be the positive time axis, the plots of the cumulative probability were transformed from the f_n domain to the $1/f_n$ mean-free time domain before applying the Weibull distribution function to $F(1/f_n)$ in order to investigate the slow events associated with dominant pitting corrosion in more detail according to the stochastic theory [31].

The Weibull probability plots for the weld metals were plotted using the PSD values as well as standard deviation values (Fig. 5a and b). The data in these plots could be fitted to two straight lines satisfactorily. In an earlier work [17,34], it was reported that the slopes in the relatively lower $1/f_n$ region were associated with the dominant uniform corrosion (in the passive state) or passivation, whereas the slopes in the relatively longer $1/f_n$ region were associated with the dominant pitting corrosion for the latter was a slow process. This method was found to be useful in distinguishing the pitting corrosion events from the passivation events in a practical way [17,34]. The intersection point of the two straight lines gives the mean-free time of the initiation of pitting corrosion. The mean-free time values obtained by PSD as well as standard deviation values of the shot-noise parameters are presented in Table 4. The values in both the columns show an excellent correlation

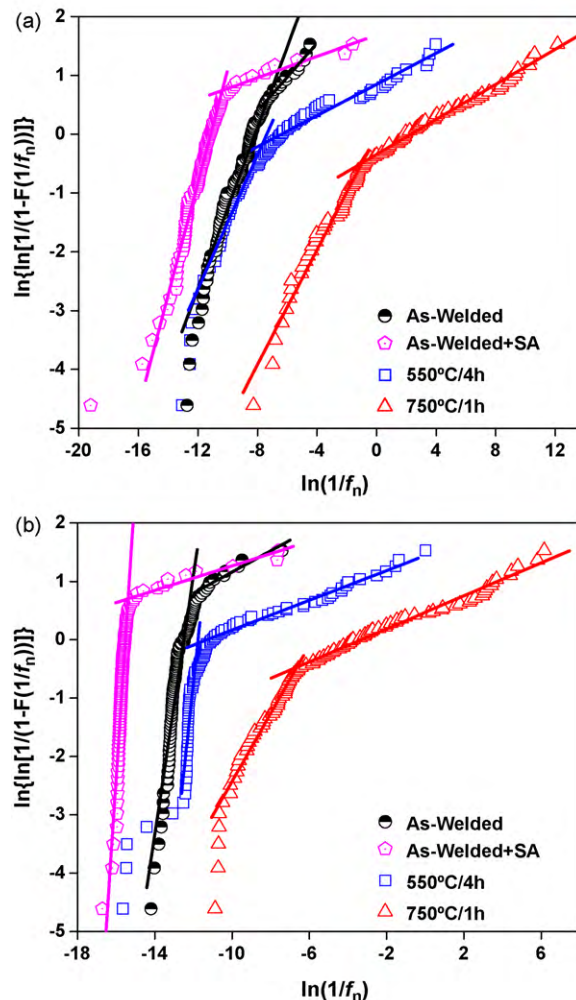


Fig. 5. Weibull probability plots for the weld metals prepared using PSD values (a) and standard deviation values (b).

Table 4
Mean-free time for pit initiation for the weld metals in aerated 0.5 M NaCl.

Weld metal specimen	Mean-free time using PSD values (s)	Mean-free time using standard deviation values (s)
As-welded	5.433×10^{-04}	5.439×10^{-06}
As-welded + SA	3.121×10^{-05}	1.898×10^{-07}
550 °C to 4 h	4.906×10^{-04}	7.431×10^{-06}
750 °C to 1 h	3.026×10^{-01}	1.096×10^{-03}

Correlation coefficient of the values in the above two columns = 0.999.

as can be seen from the correlation coefficient value of 0.999. Thus, it is observed from Table 4 that as-welded and solution-annealed specimens were relatively superior in pitting corrosion resistance.

The values of B which are used in calculating f_n and q were determined from the potentiodynamic polarisation curves and were found to be different for different weld metals (Table 3). If lower values of B increased the q values it decreased the f_n values simultaneously; thus, it is not advisable to use the 0.026 V value for B .

The cumulative probability of frequency of events, $F(f_n)$ was plotted against the frequency of events, f_n and $F(q)$ was plotted against q (Fig. 6a and b). Localized corrosion, such as pitting, can be characterized by a small number of events, and is therefore expected to have a low frequency and high charge [20]. In the case of passivity, the charge is expected to be low, while the frequency will depend on the processes occurring on the passive film [20]. It has been reported that when the cumulative probability plots do

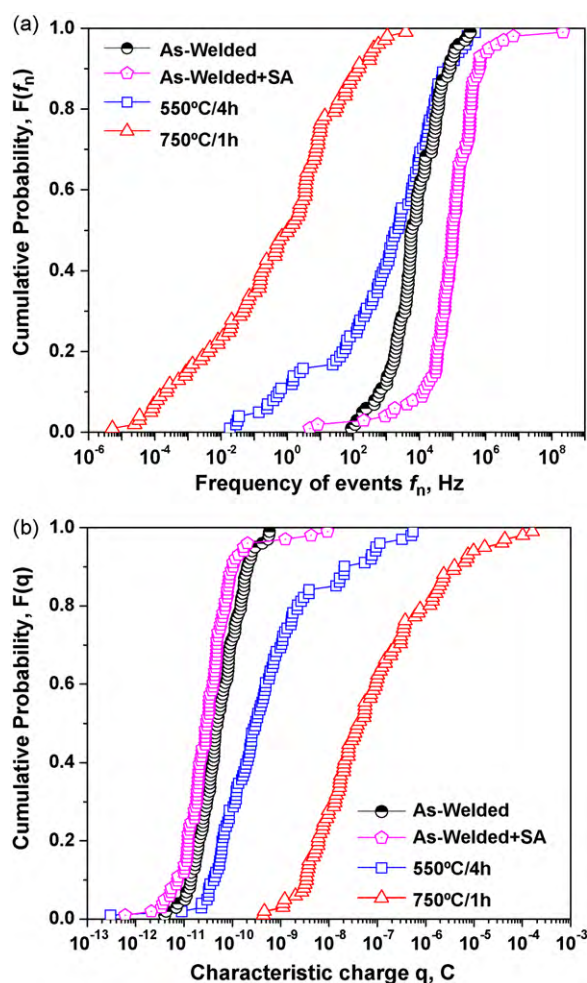


Fig. 6. Cumulative probability for the frequency of events, f_n (a) and characteristic charge, q (b) calculated using PSD values.

not overlap then it shows that there is good discrimination ability and effectiveness in the parameter studied [18]. It was reported that the cumulative probability plot in the lower cumulative probability range corresponded to dominant pitting corrosion [17]. Thermally aged weld metal specimens showed the lowest values of the f_n at the lower cumulative probabilities and in general higher values of q which indicated their increasing vulnerability towards pitting corrosion with increase in ageing temperature.

3.2. Pyramidal plots of shot-noise parameters

It has been reported that the parameters q and f_n derived from shot-noise theory provide vital information about the nature of the corrosion processes [19,23]. Thus, q gives an indication of the mass of the metal lost in the event while f_n provides information about the rate at which these events are happening [18]. During pitting a small number of events (the probability of the localized corrosion events decreases with increasing vulnerability of the alloy) with higher charge values are expected [20]. The notably used statistical parameter to extract the significant information from the EN data is the noise resistance (R_N) which is given by σ_V/σ_I where σ_I is the standard deviation of current and σ_V is the standard deviation of potential. In fact, R_N values are considered to be more helpful in studying the deterioration of the passive film than possibly the coefficient of variation of current (CVC) and the pitting index (PI). Although R_N is strictly inversely proportional to the corrosion rate only in the particular case of uniform corrosion under activation control, it is generally accepted that high R_N values are associated to low activity [18]. Thus, R_N values could be used to indicate the high or low corrosion activity. Thus, these 3D plots have f_n , R_N and q plotted on X, Y and Z axes respectively with same limits for the sake of comparison (Fig. 7a–d). The pyramidal plots of the as-welded and as-welded and solution-annealed specimens are quite different from those of the aged weld metals; it was observed that in the former case, the bases of the pyramid were well defined; however, the apexes were not well defined. This could be explained from the fact that the number of events with higher q values was absent, thus making the pyramids appear flat at the top. This is attributed to the fact that the passive alloys in general, showed events with higher frequency having higher R_N values. On the contrary, in the case of the latter, the pyramid appeared to be well-formed with the sharp apexes (more so in case of the weld metal aged at 750 °C to 1 h), owing to the fact that there were many events with lower frequency having higher q values. Shrinking the limits of the frequency axis as well as the shifting the frequency axis limit to very a low value are good indicators suggesting the pitting corrosion attack. Thus, it could be surmised that constructing a pyramid using the shot-noise parameters in conjunction with the R_N values could provide quick information about the localized corrosion aspect of the alloy under study.

3.3. Microstructural analysis

In order to reveal the location of the pitting corrosion attack on the as-welded and heat-treated specimens, anodic polarisation experiments were carried out on the freshly polished specimens,

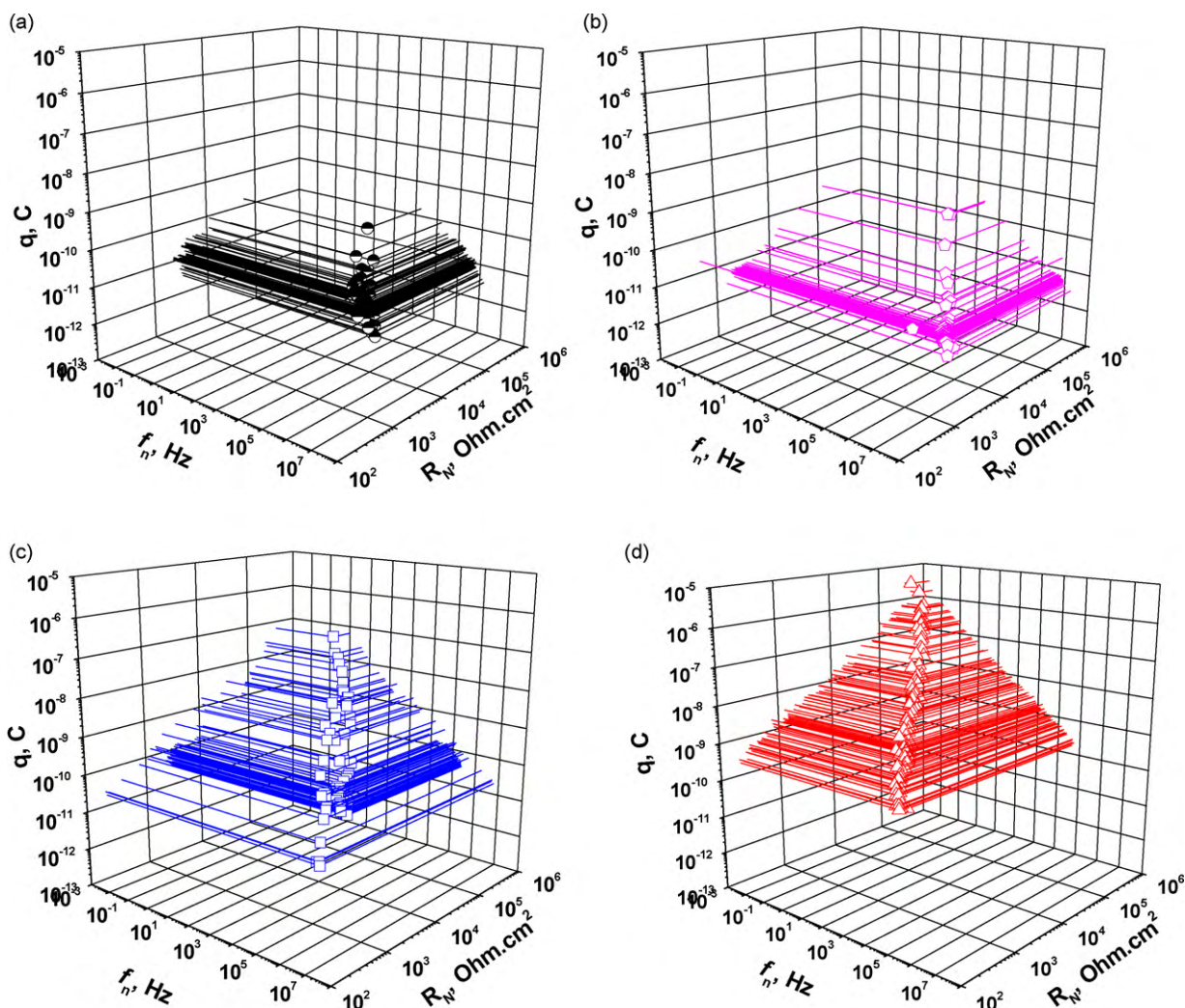


Fig. 7. 3D plots of shot-noise parameters (q and f_n) along with R_N for as-welded (a), as-welded + SA (b), 550 °C to 4 h (c) and 750 °C to 1 h (d) immersed in 0.5 M NaCl.

such that after the onset of stable pitting the anodic current was allowed to reach only up to 200 μA . After the anodic polarisation experiments, as-welded specimen was etched in Murakami reagent (10 g Potassium Ferricyanide + 10 g Potassium Hydroxide + 100 ml water, immersion in the boiling solution for 3 min), which etches the delta-ferrite and the heat-treated specimens were etched in Modified Murakami reagent. Fig. 8 shows the photomicrograph of the as-welded specimen showing a pit which was nucleated at the austenite centre and spread around the delta-ferrite; an undissolved delta-ferrite stringer is seen inside the pit. During the onset of pitting corrosion, pits generally nucleated at the austenite centres, where the Cr and Mo concentrations were the least. This is on account of the fact that Mo and Cr segregate at the δ/γ boundary during the solidification and cooling of the weld metals. Cieslak and Savage [9] reported that the extent of microsegregation was much higher for Mo than Cr in the welds where solidification mode was primary austenite compared to the welds where ferrite was the primary mode of solidification. Garner [5] too reported that the microsegregation of Mo in 316L welds was found to be almost double at the δ/γ boundary than that of the parent metal. Thus, in the present case it was obvious that, on account of the austeno-ferritic mode of solidification the microsegregation of Cr and Mo at the δ/γ boundary resulted in the impoverishment of these two elements at the austenite centres, making them susceptible for the pitting corrosion attack.

Fig. 9a and b shows the photomicrographs of 550 °C to 4 h and 750 °C to 1 h specimens after the potentiodynamic anodic polarisation experiment; in order to know the sites of pit nucleation the anodic current was restricted up to 200 μA . Thus very small pits were observed on these specimens. A pit nucleated at the bound-

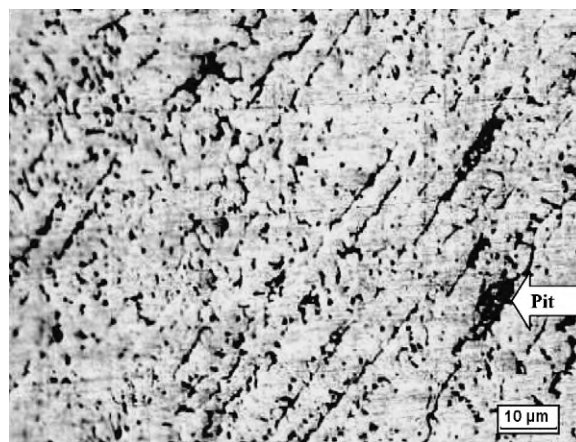


Fig. 8. Photomicrograph of the as-welded specimen after potentiodynamic anodic polarisation in aerated 0.5 M NaCl solution showing pitting corrosion attack. Etched in Murakami reagent.

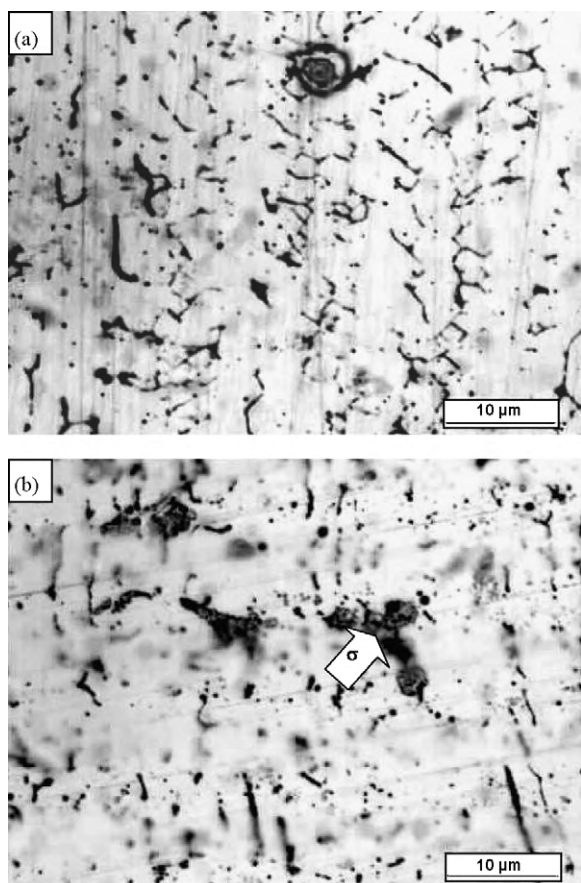


Fig. 9. Photomicrographs of the 550 °C to 4 h (a) and 750 °C to 1 h (b) specimens after potentiodynamic anodic polarisation in aerated 0.5 M NaCl solution showing pitting corrosion attack. Etched in Modified Murakami reagent.

ary of the delta-ferrite and austenite was observed in 550 °C to 4 h (Fig. 9a). Since some $M_{23}C_6$ carbides were observed at the δ/γ boundary in this specimen, the pit nucleation site would be in the region depleted of Cr. The photomicrograph (Fig. 9b) for the specimen heat-treated at 750 °C to 1 h shows a large part of the some of the delta-ferrite stringers had transformed into sigma phase and pits had nucleated in the vicinity of these phases which was depleted of Cr and Mo and had transformed into secondary austenite subsequently (Fig. 9b). This could be explained from the fact that at this temperature $M_{23}C_6$ carbide precipitation was not possible as this temperature falls beyond the upper boundary of the time temperature sensitization (TTS) diagram established for this steel [35]. At this temperature, delta-ferrite predominantly transforms to sigma phase. Any carbide precipitation that is observed is likely to have already formed during multipass welding, as it does not redissolve at this temperature. It was noticed that the pitting attack seemed to have grown inside the transformed delta-ferrite stringers attacking the secondary austenite which was transformed from the alloying-element depleted delta-ferrite; thus, in the large grown pits, sigma phase particles transformed from the delta-ferrite stringers were seen intact. The precipitates are formed by solid state diffusion, thus allowing a redistribution of chemical elements among different phases. Consequently, the elemental partition, pitting resistance equivalent (PRE) index ($PRE = \% Cr + 3.3\% Mo + 16\% N$ gives the resistance of the alloy to pitting corrosion) and corrosion resistance of each phase is different [36]. Since sigma phase is rich in Cr and Mo it had high PRE compared to the secondary austenite, therefore it did not undergo pitting attack and was seen to be intact while the pits grew around it. Since this process was

enhanced at 750 °C to 1 h, it showed most inferior pitting corrosion resistance. Pujar et al. [16] reported similar results from their work on the 316 SS weld metal (C 0.059 wt.% and N 0.053 wt.%) heat-treated at 750 °C to 5 h; the deterioration of pitting corrosion resistance of the weld metal in 0.5 M sulphuric acid + 0.5 M sodium chloride as well as in 0.5 M sodium chloride solutions in comparison with the base metal was attributed to the precipitation of $M_{23}C_6$, sigma and chi phases from the delta-ferrite and the resultant alloying-element depletion.

In the case of the solution-annealed specimen, the delta-ferrite got completely dissolved, thus leading to the formation of the single phase austenite with 0.13% N. Inhomogeneity present in the as-welded specimen was completely removed in the solution-annealed specimen resulting in a completely homogeneous microstructure devoid of any second-phase particles as well as microsegregation. The passive film on such a homogeneous microstructure would be more resistant to the pitting corrosion attack.

Thus, among all the heat-treatments that have been formulated for the PFBR welds, the ones conducted at 750 °C to 1 h and to some extent 550 °C to 4 h would be the most deleterious in terms of the pitting corrosion attack, provided the welds with these heat-treatments encountered the aqueous solution with chloride ingress into it. The solution-annealing treatment was found to restore and improve the pitting corrosion resistance of the material.

4. Conclusions

Pitting corrosion studies on the 316N weld metals in as-welded and thermally aged conditions were carried out and following conclusions were arrived at.

1. The pitting corrosion resistance degraded with increase in the temperature of ageing owing to the secondary precipitation from the delta-ferrite into $M_{23}C_6$ carbides and sigma phases resulting in the alloying-element depleted regions; in this respect, the heat-treatment at 750 °C to 1 h was found to be the most deleterious.
2. Weibull probability plots were used to determine the mean-free time values for the initiation of pitting corrosion using PSD as well as standard deviation values; mean-free time values obtained using PSD as well as standard deviation values showed excellent correlation.
3. Instead of using the commonly used shot-noise parameters like f_n , and q independently, pyramidal plots of f_n , q and R_N were constructed for quick qualitative analysis of the pitting corrosion status of the alloy.

References

- [1] S.K. Ray, V. Shankar, V. Balasubramaniam, V.K. Sethi, Heat treatment of austenitic stainless steel components, in: Proceedings of the Seminar Materials R&D for PFBR, January 1–2, 2003, p. 215.
- [2] ASM committee on Heat Treating, Metals Hand Book, 9th ed., ASM, Metals Park, OH, 1981, p. 647.
- [3] F.C. Brautigam, Welding practices that minimize corrosion, Chem. Eng. 84 (Pt. 2) (1977), pp. 97–98, 100, 102.
- [4] M.A. Streicher, Theory and Application of Evaluation Tests for Detecting Susceptibility to Intergranular Attack in Stainless Steels and Related Alloys—Problems and Opportunities, ASTM STP 656, American Society for Testing and Materials, Philadelphia, USA, 1978, p. 70.
- [5] A. Garner, Corrosion 35 (1979) 108.
- [6] O. Hammar, U. Svenson, Influence of steel composition on segregation and microstructure during solidification of austenitic stainless steels, in: Solidification and Casting of Metals, The Metals Society, London, 1979, p. 401.
- [7] R.A. Farrar, Influence of microsegregation on phase transformations and properties of type 316 weld metals at elevated temperatures, in: Stainless Steels'84, The Institute of Metals, 1 Carlton House Terrace, London SW1Y 5DB, UK, 1986, pp. 336–342.

- [8] M. Lindenmo, Microstructural factors affecting pitting resistance of weld metal of highly alloyed austenitic stainless steels, in: *Stainless Steels'84*, The Institute of Metals, 1 Carlton House Terrace, London SW1Y 5DB, UK, 1986, pp. 262–270.
- [9] M.J. Cieslak, W.F. Savage, *Weld. J.* 60 (1981) 131s.
- [10] T.G. Davey, T.G. Gooch, J.L. Robinson, *Met. Construct.* 19 (1987) 431–435.
- [11] F.C. Hull, *Weld. J.* 46 (1967) 399s.
- [12] A. Garner, *Met. Prog.* 127 (1985) 31–34.
- [13] K.F. Krysiak, *Cause and Prevention of Unusual Failures of Materials*, Corrosion/83, National Association of Corrosion Engineers, 1983, p. 16.
- [14] M. Henthorne, *Corrosion* 30 (1974) 39.
- [15] T.G. Gooch, *Weld. Inst. Res. Bull.* 15 (1974) 183.
- [16] M.G. Pujar, U. Kamachi Mudali, R.K. Dayal, T.P.S. Gill, *Corrosion* 48 (1992) 579.
- [17] K.-H. Na, S.-I. Pyun, H.-P. Kim, *Corros. Sci.* 49 (2007) 220.
- [18] J.M. Sanchez-Amaya, R.A. Cottis, F.J. Botana, *Corros. Sci.* 47 (2005) 3280.
- [19] R.A. Cottis, *Corrosion* 57 (2001) 265.
- [20] H.A.A. Al-Mazeedi, R.A. Cottis, *Electrochim. Acta* 49 (2004) 2787.
- [21] R.A. Cottis, M.A.A. Al-Awadhi, H. Al-Mazeedi, S. Turgoose, *Electrochim. Acta* 46 (2001) 3665.
- [22] A. Valor, F. Caleyo, L. Alfonso, D. Rivas, J.M. Hallen, *Corros. Sci.* 49 (2007) 559.
- [23] S.-I. Pyun, E.-J. Lee, *Surf. Coat. Technol.* 62 (1993) 480.
- [24] N. Suuataala, *Met. Trans.* 14A (1983) 191.
- [25] W.T. DeLong, *Weld. J.* 53 (1974) 273s.
- [26] D.J. Kotecki, T.A. Siewert, *Weld. J.* 71 (1992) 171s.
- [27] K. Rajasekhar, C.S. Harendranath, R. Raman, S.D. Kulkarni, *Mater. Characterization* 38 (1997) 53.
- [28] G. Gonzalez-Rodriguez, V.M. Salinas-Bravo, E. Garcia-Ochoa, A. Diaz-Sanches, *Corrosion* 53 (1997) 693.
- [29] G.A. Henshall, *J. Nucl. Mater.* 195 (1992) 109.
- [30] J.F. Chen, W.F. Bogaerts, *Corrosion* 52 (1996) 753.
- [31] K.-H. Na, S.-I. Pyun, *Corros. Sci.* 50 (2008) 248.
- [32] T. Zhang, X. Liu, Y. Shao, G. Meng, F. Wang, *Corros. Sci.* 50 (2008) 3500.
- [33] T. Zhang, C. Chen, Y. Shao, G. Meng, F. Wang, X. Li, C. Dong, *Corros. Sci.* 53 (2008) 7921.
- [34] K.-H. Na, S.-I. Pyun, *J. Electroanal. Chem.* 596 (2006) 7.
- [35] N. Parvathavarhini, R.K. Dayal, H.S. Khatak, V. Shankar, R. Shanmugam, *J. Nucl. Mater.* 355 (2006) 68.
- [36] I.N. Bastos, R.P. Nogueira, *Mater. Chem. Phys.* 112 (2008) 645.